iScience

CellPress
OPEN ACCESS

Article

The sphingosine kinase 1 activator, K6PC-5, attenuates Ebola virus infection

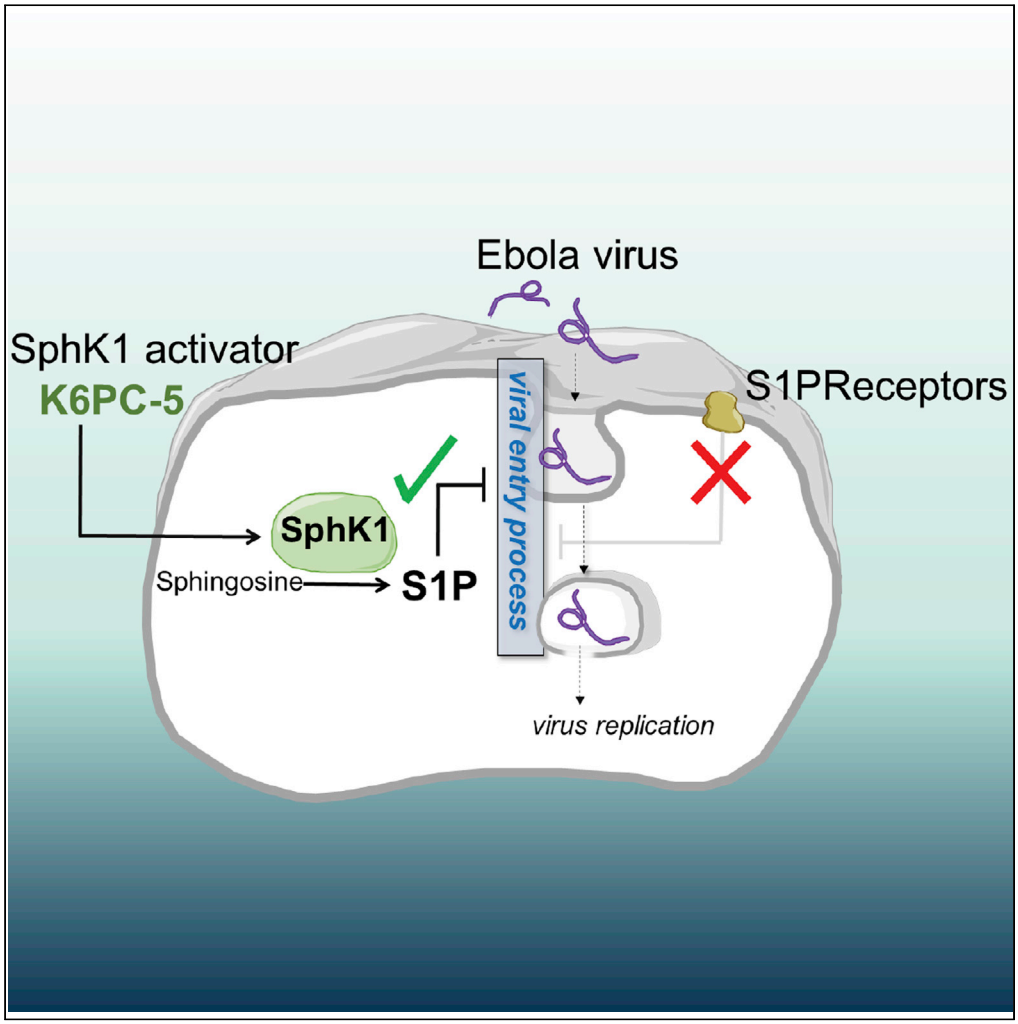

Gergely Imre, Verena Krähling, Madeleine Eichler, ..., Stephan Becker, Dagmar Meyer zu Heringdorf, Josef Pfeilschifter

gimre80@gmail.com

HIGHLIGHTS

K6PC-5, a sphingosine kinase 1 activator, inhibits Ebola virus infection

Sphingosine 1-phosphate, the product of SphK1, attenuates the viral entry

Inhibiton/activation of S1P receptors has no influence on Ebola virus entry

These data support the endogen effect of S1P in Ebola virus infection

Imre et al., iScience *24*, 102266
April 23, 2021
https://doi.org/10.1016/j.isci.2021.102266

iScience

CellPress
OPEN ACCESS

Article

The sphingosine kinase 1 activator, K6PC-5, attenuates Ebola virus infection

Gergely Imre,[1,11,*] Verena Krähling,[2,3] Madeleine Eichler,[1] Sandra Trautmann,[4] Nerea Ferreirós,[4] M. Javad Aman,[5] Fatah Kashanchi,[6] Krishnaraj Rajalingam,[7] Stefan Pöhlmann,[8,9] Stephan Becker,[2,3] Dagmar Meyer zu Heringdorf,[1,10] and Josef Pfeilschifter[1,10]

SUMMARY

Ebola virus (EBOV) is responsible for outbreaks with case fatality rates of up to 90% and for an epidemic in West Africa with more than ten thousand deaths. EBOV glycoprotein (EBOV-GP) is the only viral surface protein and is responsible for viral entry into cells. Here, by employing pseudotyped EBOV-GP viral particles, we uncover a critical role for sphingolipids in inhibiting viral entry. Sphingosine kinase 1 (SphK1) catalyzes the phosphorylation of sphingosine to sphingosine 1-phosphate (S1P). The administration of the SphK1 activator, K6PC-5, or S1P, or the overexpression of SphK1 consistently exhibited striking inhibitory effects in EBOV-GP-driven entry in diverse cell lines. Finally, K6PC-5 markedly reduced the EBOV titer in infected cells and the de novo production of viral proteins. These data present K6PC-5 as an efficient tool to inhibit EBOV infection in endothelial cells and suggest further studies to evaluate its systemic effects.

INTRODUCTION

Ebola virus disease (EVD) is a serious hemorrhagic disease caused by Zaire Ebola virus (EBOV) infection (case fatality rate is up to 90%). EBOV is a member of the *Filoviridae* family. The genus ebolavirus includes six species, three of which contain members that are highly pathogenic in humans (Pourrut et al., 2005) including EBOV (2014–2016 epidemic and 2018–2020 outbreak). The initial flu-like symptoms are followed by the occurrence of gastro-intestinal symptoms and hemorrhage (Ansari, 2014; Fauci, 2014). To date, despite some recent success with immunotherapy (Levine, 2019) effective causal treatment of EVD is not available, although supportive care can increase the chance of survival significantly (Wolf et al., 2014). Furthermore, a vaccine against EVD has been successfully tested and approved in 2019 (Ollmann Saphire, 2020), which offers an effective measure to prevent this lethal infectious disease. In contrast, efforts to develop robust pharmacological methods as therapeutic possibilities are limited. The loss of endothelial barrier function in blood vessels and the subsequent bleeding is considered as one of the major pathogenic factors of this serious infectious disease. This phenomenon may be in part due to a drastically elevated cytokine response (Escudero-Pérez et al., 2014). However, infection-induced endothelial cell death may also be an important pathogenic factor, but it was not investigated in detail. EBOV comprises a single stranded genomic RNA encoding seven structural proteins with distinct functions, including viral entry, RNA synthesis and viral budding (Dolnik et al., 2008). The EBOV glycoprotein (EBOV-GP) is the only surface protein of EBOV. It forms a homo-trimer and is required for viral entry into cells (Sanchez et al., 1998). Besides, EBOV-GP is suggested to trigger the so far poorly understood cytopathic effect of EBOV. Previously, it has been demonstrated that ectopic expression of EBOV-GP results in rounding up of the cells and leads to loss of cytoplasm-membrane integrity in different cell types (Volchkov et al., 1998).

Apoptosis and necrosis are two distinct forms of cell death. Apoptosis is an intensively studied cell death modality. Morphologically it is characterized by cell shrinkage, condensation and fragmentation of the nuclei and fragmentation of the nucleosomal DNA (Wyllie, 1987). Apoptosis is regulated by a family of cysteine proteases, termed caspases. Structurally and functionally, apoptotic caspases are divided into two categories: initiator caspases (caspase-8 and -9) and effector caspases (caspase-3 and -7) (Mace and Riedl, 2010). In contrast, necrosis is characterized by early membrane rupture of the cells. In the past decades, it became evident that necrotic-like cell death modalities can be also considered as a regulated

[1]Institute of General Pharmacology and Toxicology, University Hospital Frankfurt, Goethe University Frankfurt, Frankfurt am Main 60590, Germany

[2]Institute of Virology, Philipps University Marburg, Marburg, Germany

[3]German Center for Infection Research (DZIF), partner site Gießen–Marburg–Langen, Marburg, Germany

[4]Institute of Clinical Pharmacology, University Hospital Frankfurt, Goethe University Frankfurt, Frankfurt am Main 60590, Germany

[5]Integrated BioTherapeutics, Inc., Gaithersburg, MD 20850, USA

[6]Laboratory of Molecular Virology, George Mason University Manassas, VA 20110, USA

[7]Cell Biology Unit, University Medical Center of the Johannes Gutenberg University Mainz, 55131 Mainz, Germany

[8]Infection Biology Unit, German Primate Center - Leibniz Institute for Primate Research, 37077 Göttingen, Germany

[9]Faculty of Biology and Psychology, University Göttingen, 37077 Göttingen, Germany

[10]These authors contributed equally

[11]Lead contact

*Correspondence: gimre80@gmail.com

https://doi.org/10.1016/j.isci.2021.102266

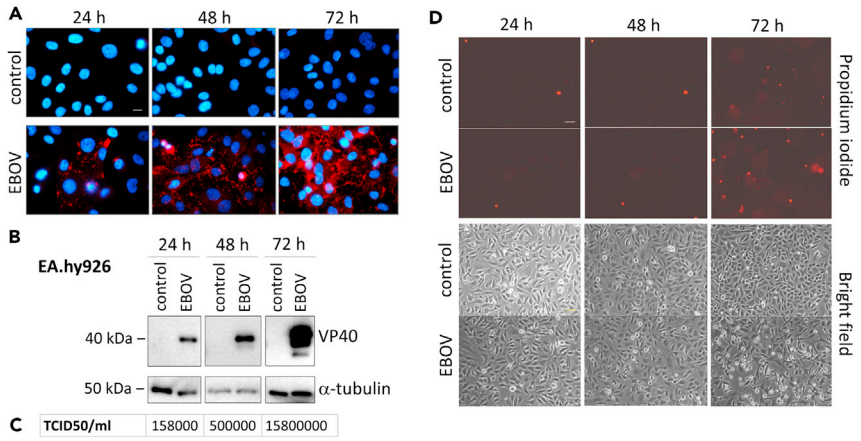

Figure 1. EBOV infection and EBOV-induced cytopathic effect in endothelial cells

(A) Fluorescence microscopy of DAPI (blue) and anti-VP40 (Alexa 594/red) stained EA.hy926 cells 24–72 hr after EBOV infection (MOI = 1). Scale bar: 10μm.

(B) Immunoblot of VP40 viral matrix protein 24-72 hr after EBOV infection in EA.hy926 cells (MOI = 1).

(C) Determination of viral titer by TCID50 assay 24–72 hr after EBOV infection in EA.hy926 cells (MOI = 1).

(D) Fluorescence microscopy of propidium iodide stained EA.hy926 cells 24–72 hr after EBOV infection (MOI = 1). Scale bar: 50μm.

process (Vanden Berghe et al., 2014) and that they play a crucial role in response to various virus infections (Imre, 2020).

Sphingolipids, defined by their sphingoid base backbone, comprise a multitude of diverse chemical structures with distinct biological functions (Hannun and Obeid, 2018a, 2018b). In particular, ceramide and sphingosine 1-phosphate (S1P) appear to be involved in the regulation of cell growth, cell death and survival (Newton et al., 2015). The cellular equilibrium between S1P and ceramides has been named the sphingolipid rheostat, in which generally pro-apoptotic ceramides counterbalance pro-survival S1P (Newton et al., 2015). S1P is formed from sphingosine by sphingosine kinases (SphK) (Hannun and Obeid, 2018a, 2018b). The two isoforms of SphK differ in subcellular localization, regulation, and biological functions (Hatoum et al., 2017; Pyne et al., 2018). Particularly SphK1 promotes cell growth and activates pro-survival pathways, but also SphK2 plays a role in growth of certain cancers (Hatoum et al., 2017). S1P can both act intracellularly or be exported and activate specific G-protein-coupled S1P receptors (S1P-GPCR), S1P1-5 (Obinata and Hla, 2019). S1P-GPCRs play important roles in inflammation, for example, by regulating lymphocyte trafficking and other immune cell functions and by maintenance of the vascular endothelial barrier (Obinata and Hla, 2019).

Sphingolipids play multiple roles in viral infection by regulating both host defense mechanisms and viral replication (Schneider-Schaulies and Schneider-Schaulies 2015; Bezgovsek et al., 2018). Acid sphingomyelinase has been implicated in EBOV attachment (Miller et al., 2012), however, the role of the S1P signaling system in EBOV infection remains largely unknown. In this report, we demonstrate an unexpected role for K6PC-5, a pharmacological SphK1 activating compound in attenuating the EBOV infection.

RESULTS

EBOV infects EA.hy926 cells and facilitates EBOV-GP-dependent necrotic cell death

It has been previously demonstrated that various endothelial cell lines are permissive to EBOV infection (Geisbert et al., 2003). Along with this, we infected EA.hy926 endothelial-like cells with EBOV. The immunofluorescence analysis of the EBOV matrix protein VP40 and the Western blot analysis of the infected cells demonstrated a continuous multiplication in the number of infected cells from 24 to 72 hr post-infection (Figures 1A and 1B). The increase in infectious viral particles in the supernatant of the cells was confirmed by tissue culture infectious dose 50 (TCID50) assays (Figure 1C). Intriguingly, a subpopulation of the infected cells exhibited morphological changes as rounding up and membrane integrity loss detected by propidium iodide staining 72 hr after infection (Figure 1D).

The detected loss of membrane integrity may indicate either the involvement of necrosis or the presence of post-apoptotic secondary membrane rupture. Therefore, to study the involvement of apoptosis in this process, we have monitored the cleavage of the apoptotic caspase substrate PARP (Tewari et al., 1995) in EA.hy926 cells. However, EBOV infection did not cause a substantial PARP cleavage in the cells (Figures 4B and 4C). In order to exclude the involvement of apoptotic caspases in the infection process, the EBOV-infected cells were treated with the pan-caspase inhibitor z-VAD-fmk (zV). The caspase inhibitor did not exhibit an inhibitory effect on the virus infection monitored by VP40 detection in EA.hy926 cells (Figure S1A) and did not block EBOV-triggered necrosis (Figure S1B). It is of note that the necrotic cell death was amplified by the addition of zV both in the absence and presence of EBOV (Figure S1B). This data are in concordance with a previous study on human macrophages, where the induction of a non-apoptotic, necrotic cell death was proposed in response to EBOV infection (Olejnik et al., 2013). Necroptosis is a regulated form of necrotic cell death, which is conducted by receptor-interacting serine/threonine protein kinases (Christofferson and Yuan, 2010) and the effector molecule mixed lineage kinase domain-like pseudokinase (MLKL), which oligomerizes and forms a pore throughout the cell membrane (Sun et al., 2012). To study the involvement of necroptosis in EBOV infection, we employed the MLKL inhibitor necrosulfonamide (NSA) alone or in combination with zV. Importantly, the treatment with NSA had no inhibitory effect, neither on the VP40 level (Figure S1A) nor on the EBOV-induced necrosis (Figure S1B), which indicates that EBOV infection triggers a necrotic-like cell death distinct from necroptosis in endothelial cells.

Previously, EBOV-GP has been suggested as the viral protein responsible for the cytopathic effect of EBOV (Simmons et al., 2003). To investigate the role of EBOV-GP, we ectopically expressed EBOV-GP in EA.hy926 cells. The expression of the viral glycoprotein (Figure S2A) resulted in significantly increased necrotic cell death characterized by membrane integrity loss detected by flow cytometry (Figure S2B). In contrast, signs of apoptosis as DNA fragmentation (Figure S2C) or phosphatidylserine externalization (Annexin V positivity) were undetectable (Figure S2D) in the EBOV-GP expressing cells. Intriguingly, the ectopic expression of two other structural viral proteins nucleoprotein (EBOV-NP) and EBOV-VP40 did not result in significant necrosis, indicating a specific role for EBOV-GP in this necrotic process (Figure S2E). In addition, increase in necrotic cell death was observed after the administration of recombinant EBOV-GP lacking the transmembrane domain (Figure S2F), suggesting that the cytotoxic potential of EBOV-GP is not exclusively due to overexpression-triggered cell death events. These results indicate the existence of an EBOV infection-induced non-apoptotic cell death, which is possibly triggered by EBOV-GP.

Murine leukemia virus-EBOV-GP pseudotyped virions efficiently transduce multiple human cell types

EBOV-GP as the only surface protein conducts both host recognition and viral entry processes (Sanchez et al., 1998). In order to further determine the role of EBOV-GP in the virus infection, we established a murine leukemia virus (MLV)-based pseudotyped virus system (Bartosch et al., 2003). We generated replication incompetent virions containing RNA encoding luciferase (Luc) and exhibiting EBOV-GP on the surface (Figure 2A). Importantly, the MLV-EBOV-GP virions efficiently transduced endothelial-like EA.hy926 (Figures 2B and 2C), epithelial HeLa (Figure 2D), and endothelial HMEC-1 (Figure 2E) cells, monitored by luciferase activity detection 24–48 hr post-infection. In contrast, MLV particles lacking EBOV-GP (MLV-control) were unable to transduce the cells. These data together implicate the indispensable role of EBOV-GP in viral entry in multiple epithelial/endothelial-like cell lines.

The SphK1 activator, K6PC-5, inhibits MLV-EBOV-GP-induced viral entry

Since SphK1 is known to play a role in both cell survival and viral infection (Pyne et al., 2018; Bezgovsek et al., 2018), we wondered whether this enzyme had an impact on EBOV-induced viral infection. K6PC-5, a poorly characterized SphK1 activator (Hong et al., 2008; Ji et al., 2015), efficiently blocked hypoxia-induced necrosis in cardiac myocytes (Liu et al., 2018); however, its influence on virus infection and infection-induced necrosis has not been studied yet.

In order to evaluate its relevance in virus infection, we treated EA.hy926, HeLa and HMEC-1 cells with K6PC-5 and performed the transduction with MLV-EBOV-GP viral particles (Figures 2B–2E). Surprisingly, the MLV-EBOV-GP-induced viral entry was strikingly inhibited in the samples, where 50 μM K6PC-5 was employed. Moreover, significant inhibitory effect was achieved already at 10μM of K6PC-5 in EA.hy.926 cells (IC_{50} = 6.75μM) (Figure 2B). The role of SphK1 was further tested by ectopically expressing the enzyme before transduction of the cells. The overexpression of SphK1 (Figure 2F) resulted in a significant drop in viral entry

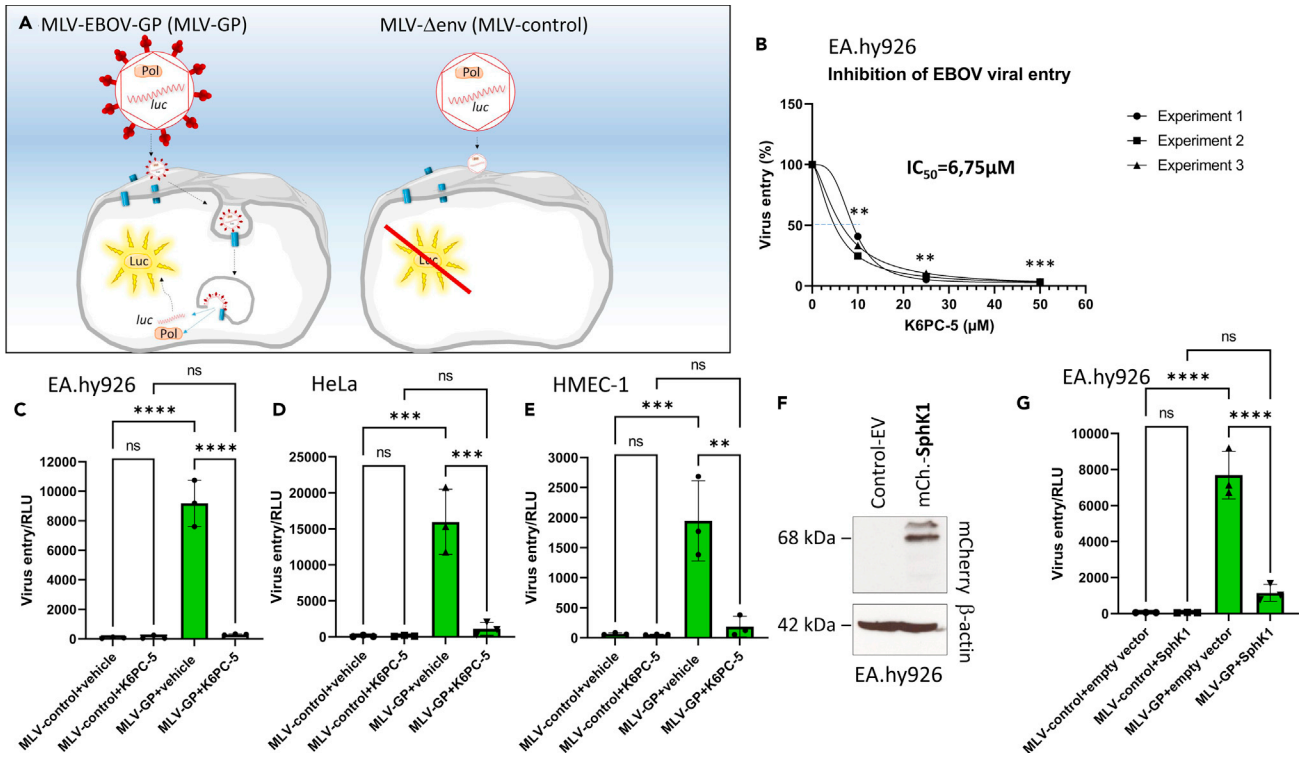

Figure 2. Infection of EA.hy926 cells with MLV-EBOV-GP pseudotyped particles is inhibited by K6PC-5

(A) Graphical representation of the mechanism of the viral entry of MLV pseudotyped particles. Pol = viral polymerase, *luc* = RNA encoding the luciferase (Luc) protein.

(B) Percentage of viral entry in MLV-EBOV-GP (MLV-GP)-infected EA.hy926 cells 24 hr post-infection. The cells were treated with vehicle (DMSO) or 10, 25, and 50 µM K6PC-5, respectively, 1 hr before and immediately after transduction. The values indicate the percentage of viral entry, measured as luciferase activity, relative to the vehicle treated samples. (means ± SD, n = 3, **p < 0.01, ***p < 0.001 in one sample t test)

(C) Luciferase activity in MLV-Δenv (MLV-control) or MLV-EBOV-GP (MLV-GP)-infected EA.hy926 cells 24 hr post infection. The cells were treated with vehicle (DMSO) or 50 µM K6PC-5 at the time of transduction. The values indicate the luciferase activity in relative luminescence unit (RLU) detected after infection with MLV without glycoprotein (MLV-Δenv) or with MLV-GP. (means ± SD, n = 3, ****p < 0.0001 in one-way ANOVA, Tukey's multiple comparisons test).

(D) Luciferase activity in MLV-Δenv (MLV-control) or MLV-EBOV-GP (MLV-GP)-infected HeLa cells 48 hr post infection. The cells were treated with vehicle (DMSO) or 50 µM K6PC-5 at the time of transduction. (means ± SD, n = 3: ***p < 0.001 in one-way ANOVA, Tukey's multiple comparisons test).

(E) Luciferase activity in MLV-Δenv (MLV-control) or MLV-EBOV-GP (MLV-GP)-infected HMEC-1 cells 24 hr post-infection. The cells were treated with vehicle (DMSO) or 50 µM K6PC-5 at the time of transduction. (means ± SD, n = 3: **p < 0.01; ***p < 0.001 in one-way ANOVA, Tukey's multiple comparisons test).

(F) Immunoblot detection of SphK1 in EA.hy926 cells transfected with pcDNA3.1 empty vector (control-EV) or pmCherry-SphK1.

(G) Luciferase activity of MLV-EBOV-GP-infected EA.hy926 cells transfected with pcDNA3.1 empty vector (control-EV) or pmCherry-C1-SphK1 (mCherry-SphK1). The values indicate the luciferase activity in relative luminescence unit (RLU) detected 24 hr after transduction. Data are presented as (means ± SD, n = 3, ****p < 0.0001 in one-way ANOVA, Tukey's multiple comparisons test).

efficiency in MLV-EBOV-GP-infected cells supporting the role of SphK1 in the inhibition of infection (Figure 2G). In contrast, the MLV-EBOV-GP-driven viral entry was not inhibited when SphK2 was overexpressed (Figures 3A and 3B) in the cells. To exclude a SphK-independent effect of K6PC-5, we generated stable SphK1 knockdown cell lines (Figure S3A). The viral entry assay was repeated by employing the SphK1 depleted cells in the presence of 25 µM K6PC-5. Of note, the inhibitory effect of K6PC-5 was significantly, yet not entirely, reduced (Figure S3B) in the SphK1 depleted cell lines. Interestingly, in spite of a significant reduction in SphK1 protein level (Figure S3A), the S1P level in the cells was only minimally and not significantly reduced (Figure S3C). This suggests either some residual SphK1 activity or a compensatory effect in response to a permanent depletion of SphK1, as previously reported by others (Allende et al., 2004).

K6PC-5 attenuates EBOV viral entry via S1P in an S1P-GPCR-independent manner

Treatment of EA.hy926 cells with 50 µM K6PC-5 significantly elevated concentrations of S1P d18:1 in the cells by about 2.5-fold, as measured by high-performance liquid chromatography-tandem mass spectrometry (Figure 3C). These results indicate the role of elevated S1P in the EBOV-GP-driven viral entry

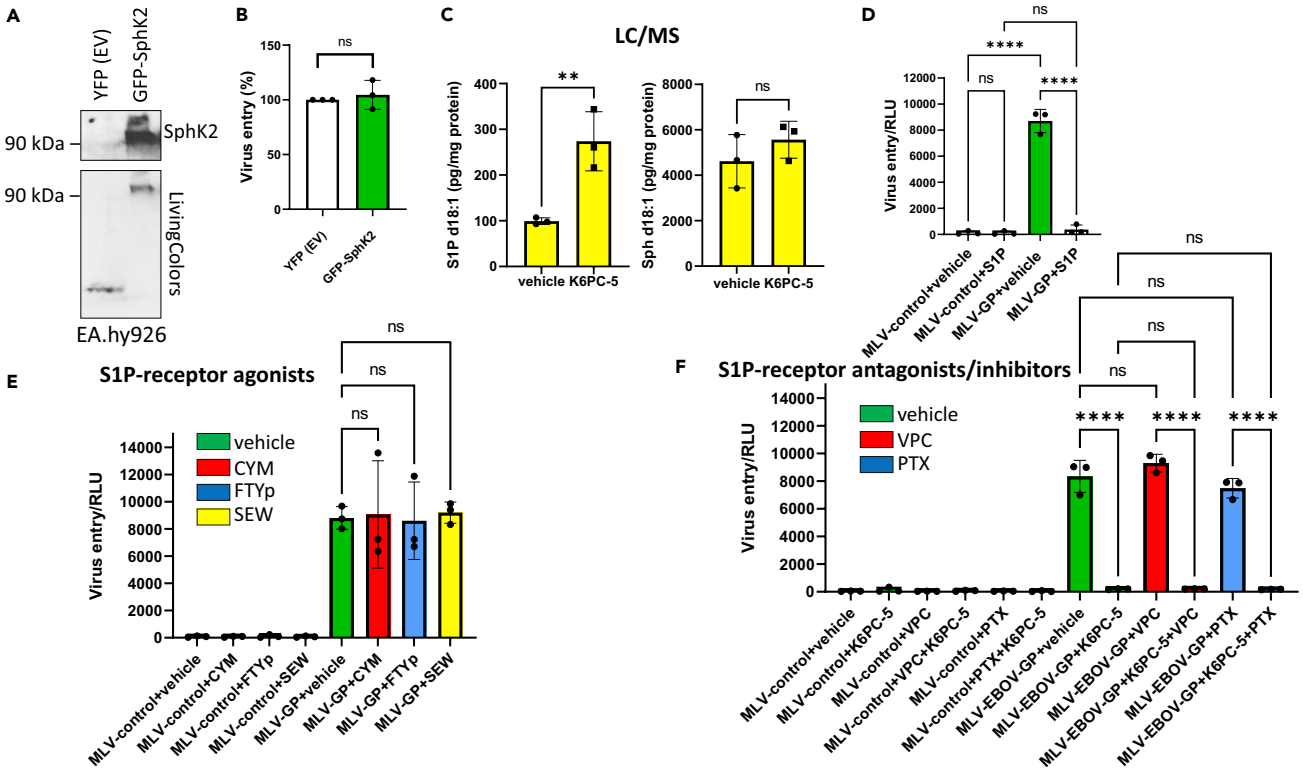

Figure 3. Transduction of EA.hy926 cells with MLV-EBOV-GP pseudotyped particles is inhibited by S1P in an S1P receptor-independent manner

(A) Western blot analysis of EA.hy926 cells transfected with pYFP empty vector (EV) or pAcGFP-C2_SphK2 (GFP-SphK2) 48 hr post transfection.

(B) Luciferase activity of MLV-EBOV-GP-infected EA.hy926 cells (24 hr). The cells were transfected with pEYFP-N1 (YFP EV) or GFP-SphK2 48 hr before transduction. The values indicate the percentage of viral entry, measured as luciferase activity, relative to control-EV samples. Data are presented as means ± SD, n = 3, ns, not significant in one sample t test.

(C) Mass spectrometry-based determination of the concentration of S1P and sphingosine (Sph) d18:1 in EA.hy926 cells 24 hr after treatment with vehicle (DMSO) or with 50 μM K6PC-5 (means ± SD, n = 3). The samples were normalized to total protein concentration. The data represent the amount of sphingoid base (pg)/mg protein. Data are presented as means ± SD, n = 3; **p < 0.01; ns, not significant in Student's t test.

(D) Luciferase activity detection (as in Figure 2C) of MLV-control or MLV-EBOV-GP (MLV-GP) transduced EA.hy926 cells 24 hr after infection. The cells were treated with vehicle (0.1% methanol and 10 μg/mL BSA) or with 1 μM S1P at the time of transduction. Data are presented as means ± SD, n = 3, ns, not significant; ****p < 0.0001 in one-way ANOVA, Tukey's multiple comparisons test.

(E) Luciferase activity detection (as in Figure 2C) of MLV-control or MLV-EBOV-GP (MLV-GP) transduced EA.hy926 cells 24 hr after infection. The cells were treated with vehicle (DMSO) or with CYM5520 (CYM) (1 μM), FTYp (1 μM) and SEW2871 (SEW) (1μM), respectively, 1 hr before and immediately after transduction. Data are presented as means ± SD, n = 3, ns, not significant in one-way ANOVA, Tukey's multiple comparisons test.

(F) Luciferase activity detection (as in Figure 2C) of MLV-control or MLV-EBOV-GP (MLV-GP) transduced EA.hy926 cells 24 hr after infection. The cells were treated with vehicle (DMSO) or with VPC23019 (VPC) (10 μM) and pertussis toxin (PTX) (100 ng/mL), respectively 2 hr before and immediately after transduction. Vehicle (DMSO) or K6PC-5 (50 μM) was added 1 hr before and immediately after transduction. Data are presented as means ± SD, n = 3, ns, not significant; ****p < 0.0001 in one-way ANOVA, Tukey's multiple comparisons test.

inhibition. In order to further confirm the role of this phosphorylated sphingolipid in viral entry inhibition, we have treated the EA.hy926 cells with S1P. The administration of 1 μM S1P d18:1 resulted in a nearly complete inhibition of viral entry detected by luciferase activity measurement (Figure 3D). It has been shown earlier that S1P could act both extra and intracellularly. S1P, once secreted, is capable to bind and activate G-protein-coupled S1P receptors (S1P-GPCRs) (Obinata and Hla, 2019). In order to test the role of S1P-GPCR activation in the EBOV entry-inhibition, we have employed various S1P receptor agonists and antagonists. The administration of S1P receptor-2 (S1P2) agonist CYM5520, the S1P1, 3, 4, and 5 agonist FTY720-phosphate (FTYp) and the S1P1 agonist SEW2871 did not exhibit significant inhibitory effects on viral entry (Figure 3E). Further, treatment with S1P receptor antagonist, VPC23019 and the inhibitor of G_I proteins, pertussis toxin (PTX), did not influence the inhibitory potential of K6PC-5 (Figure 3F). These data together are in favor of a S1P-GPCR-independent, likely intracellular effect of K6PC-5 in EBOV viral entry.

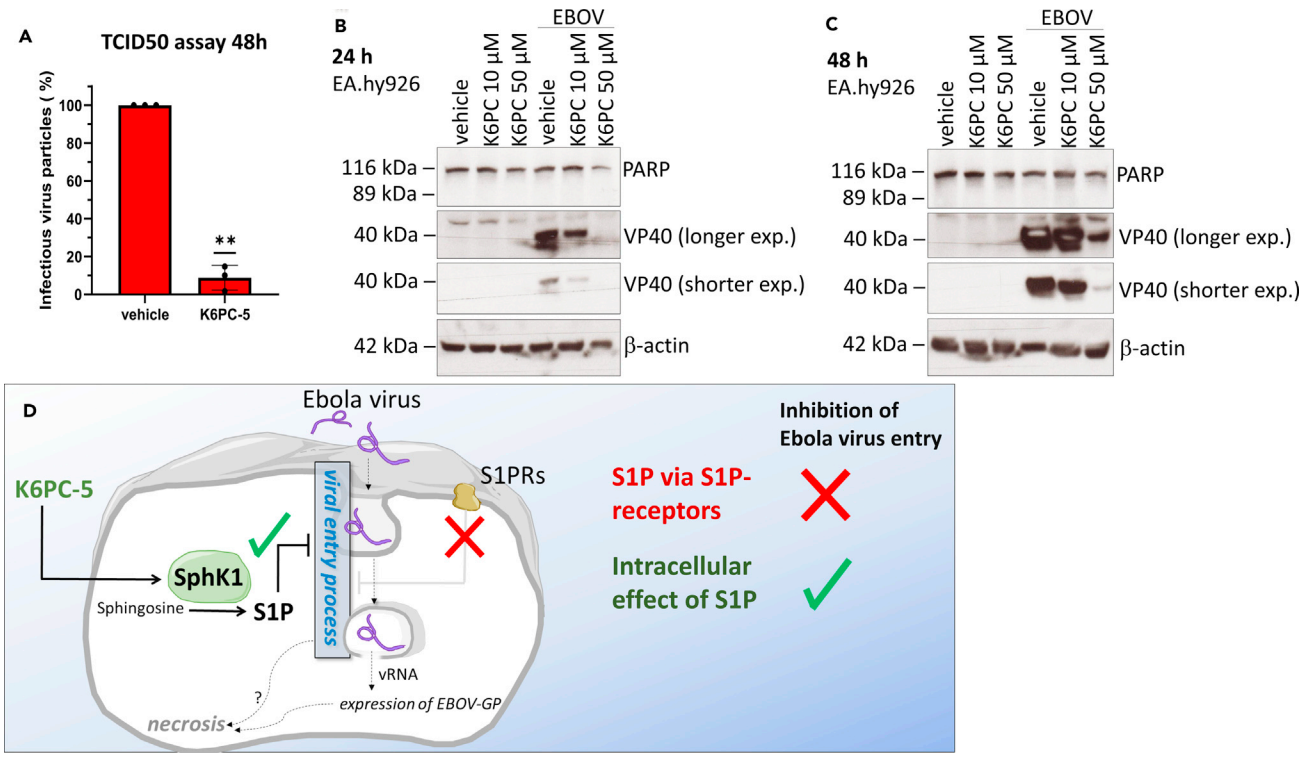

Figure 4. EBOV infection in EA.hy926 cells is inhibited by K6PC-5

(A) TCID50 assay (48 hr post infection) of EBOV-infected EA.hy926 cells treated with vehicle (DMSO) or with 50 µM K6PC-5 1 hr prior infection (n = 3). The infection is presented as percentage relative to the untreated samples (vehicle). Data are shown as means ± SD, n = 3; **p < 0.01 in one sample t test.

(B) Immunoblot of PARP cleavage and VP40 expression of EBOV-infected EA.hy926 cells (24 hr post infection) treated with vehicle (DMSO) or K6PC-5 at various concentrations (as indicated).

(C) Immunoblot of VP40 expression of EBOV-infected EA.hy926 cells (48 hr post-infection) treated with vehicle (DMSO) or K6PC-5 at various concentrations (as indicated).

(D) Graphical representation of the proposed action of K6PC-5 on EBOV infection.

K6PC-5 significantly attenuates EBOV-induced infection

Finally, to confirm the inhibitory role of K6PC-5 on EBOV infection, EA.hy926 cells were treated with K6PC-5 and infected with EBOV. The amount of infectious viral particles in the supernatants was determined by TCID50 assay. Most interestingly, K6PC-5 significantly reduced the virus titers in supernatants of infected cells (Figure 4A) and strikingly decreased the amount of VP40 in a concentration-dependent manner (Figures 4B and 4C). Thus, K6PC-5 represents an effective pharmacological tool to reduce the infectious viral titer of EBOV (Figure 4D).

DISCUSSION

In the present study, we addressed the role of SphKs in infection caused by EBOV and EBOV-GP-bearing pseudotyped virions. As being parts of the sphingolipid rheostat, SphKs promote cell survival and thus could potentially inhibit virus-induced cell death (Newton et al., 2015; Hofmann et al., 2008), and there is increasing evidence that SphKs may be important host factors that can be hijacked by certain viruses and manipulated to their advantage (Schneider-Schaulies and Schneider-Schaulies 2015).

We provided evidence that K6PC-5, a pharmacological SphK1 activator significantly reduced the extent of EBOV infection. Since K6PC-5 can function as a cell death inhibitor and exhibits pro-survival properties in diverse cell types (Shao et al., 2015; Ji et al., 2015; Liu et al., 2018), one can conclude that inhibition of the virus-induced necrosis directly leads to this significantly decreased infectious potential. However, the virus-induced necrotic cell death occurs at late time points (72–96 hr) post-infection in endothelial cell lines, which argues against the primary role of necrosis in infection control at least because of two reasons. First, only a subpopulation of cells exhibit necrosis. Second, we could detect the inhibitory effect of K6PC-5 on

virus production and viral entry at a significantly earlier time point (24 hr). This suggests that the target of K6PC-5 may act upstream of the point of necrosis initiation, and therefore we conclude that the occurrence of necrosis in the process is only a late consequence of the virus replication (Figure 4D).

It is of note that K6PC-5 provided the most prominent anti-viral effect at 50 μM concentration, which was not cytotoxic in EA.hy926 cells up to 48 hr when measured with flow cytometry (PI staining and subG1 detection, data not shown). In addition, 10 μM K6PC-5 already exhibited significant inhibitory effect and 25 μM K6PC-5 provided an almost total inhibition in EA.hy926. Previous studies have shown that K6PC-5 efficiently stimulated SphK activity in the range of 10–100 μM in various cell types (Hong et al., 2008; Ji et al., 2015; Shao et al., 2015; Liu et al., 2018). Furthermore, 50 μM K6PC-5 was used for neuroprotection in *in vitro* models of Huntington's disease (Di Pardo et al., 2017), suggesting that the concentration required for the anti-viral effect is generally well tolerated by cultured cells. Finally, daily intraperitoneal injections of 0.05 mg/kg K6PC-5 for 5 weeks in mice improved symptoms in a model of Huntington's disease and appeared to be well tolerated by the animals (Di Pardo et al., 2019).

Whether K6PC-5 activates exclusively SphK1 and not SphK2 remains unclear at present, as its effect on SphK2 has not been tested explicitly. Our data with ectopic expression of SphK2 indicate that elevated level of SphK2, surprisingly, might not play a role in viral entry (Figures 3A and 3B).

Our data indicate that K6PC-5 significantly elevates intracellular S1P and thus acts intracellularly since pharmacological manipulation of diverse S1P-GPCRs showed no influence on the anti-viral effect of K6PC-5. It is in line with a previous observation in which the intracellular effect of K6PC-5 has been shown in a keratinocyte cell line (Hong et al., 2008).

Since the genetic depletion of SphK1 did not significantly alter the S1P level in the cells, our data do not entirely exclude a role of residual SphK1 or a compensatory effect of SphK2 in the knockdown cells. This is in concordance with previous studies on SphK1 knock out mice, where in spite of the lack of SphK1 and drop in plasma level of S1P the endogenous level of S1P was not markedly reduced in multiple cell types (Allende et al., 2004). For this reason, by employing genetic depletion of SphK1, our study cannot entirely exclude that K6PC-5 also binds SphK2 or other targets than SphKs.

SphKs have been implicated in infections with diverse viruses (Carr et al., 2013; Schneider-Schaulies and Schneider-Schaulies, 2015; Bezgovsek et al., 2018; Seo et al., 2013). Inhibition of SphKs has been shown to reduce infection in Influenza A virus (Xia et al., 2018), in Measles virus (Vijayan et al., 2014) and in Chikungunya virus (Reid et al., 2015). None of the above mentioned viruses was affected by extracellular S1P (Seo et al., 2013; Reid et al., 2015; Vijayan et al., 2014). We show here that EBOV differs from the SphK dependent viruses because its replication was inhibited by a SphK1 activator and by administration of S1P. In this respect, EBOV rather resembles bovine viral diarrhea virus (BVDV) (Yamane et al., 2009). BVDV directly inhibited SphK1 via its non-structural protein, NS3, and inhibition or deletion of SphK1 strongly enhanced replication of this virus (Yamane et al., 2009). This corresponds to the inhibitory effect of SphK1 activation which we show here for EBOV. It remains an open question how SphK1 and S1P could counteract EBOV infection. The experiments with the pseudotyped virions suggest that viral entry rather than viral replication or viral budding were affected.

In conclusion, our data demonstrate a strong inhibitory effect of K6PC-5 in EBOV infection possibly via the effect on SphKs and intracellular S1P. Thus, the detailed investigation of sphingolipid metabolism in EBOV infection might be a promising starting point to develop an efficient pharmacological therapy for this serious infectious disease.

Limitations of the study

Our study was performed on human cell lines. It would be interesting to extend the study by employing *in vivo* models in order to evaluate the systemic effect of K6PC-5 and Sphks on EBOV infection.

Resource availability

Lead contact

Further information and requests for resources should be directed to and will be fulfilled by the lead contact, Gergely Imre: gimre80@gmail.com.

Material availability

This study did not generate novel unique reagents.

Data and code availability

The authors declare that all the data supporting the findings of this study are available within the article and its supplemental information files or from the corresponding author upon reasonable request.

METHODS

All methods can be found in the accompanying transparent methods supplemental file.

SUPPLEMENTAL INFORMATION

Supplemental information can be found online at https://doi.org/10.1016/j.isci.2021.102266.

ACKNOWLEDGMENTS

We thank to Stephanie Schwalm and Rajkumar Vutukuri for the valuable discussions and to Katharina Spohner and Natalie Aster for the assistance in protein concentration measurement. The project was supported by the German research foundation, Germany (DFG, SFB1039 to J.P. and D. MzH., Projekt ID:204083920), by the Uniscientia Foundation Vaduz, Lichtenstein to J.P. and by the program of Frankfurter Forschungsförderung 2016, Germany Nachwuchsforscher to G.I. (71000323). Furthermore, the study was funded by the LOEWE Center DRUID, Germany project A1 (to SB)

AUTHOR CONTRIBUTIONS

Conceptualization: G.I., D.MzH. and J.P.; investigation: G.I., V.K., M.E., S.T.; data analysis: G.I., V.K., M.E., S.T., and N.F.; writing - original draft: G.I.; writing - review and editing, G.I., J.P., and D. MzH., funding acquisition: J.P., D.MzH., and G.I.; resources: J.P., S.B., D.MzH., S.P., K.R., F.K., and M.J.A.; supervision: G.I.

DECLARATION OF INTERESTS

The authors declare no competing interest.

Received: July 7, 2020
Revised: February 8, 2021
Accepted: March 1, 2021
Published: April 23, 2021

REFERENCES

Allende, M.L., Sasaki, T., Kawai, H., Olivera, A., Mi, Y., van Echten-Deckert, G., Hajdu, R., Rosenbach, M., Keohane, C.A., Mandala, S., et al. (2004). Mice deficient in sphingosine kinase 1 are rendered lymphopenic by FTY720. J. Biol. Chem. *279*, 52487–52492, https://doi.org/10.1074/jbc.M406512200.

Ansari, A.A. (2014). Clinical features and pathobiology of Ebolavirus infection. J. Autoimmun. *55*, 1–9.

Bartosch, B., Dubuisson, J., and Cosset, F.L. (2003). Infectious hepatitis C virus pseudo-particles containing functional E1-E2 envelope protein complexes. J. Exp. Med. *197*, 633–642.

Bezgovsek, J., Gulbins, E., Friedrich, S.K., Lang, K.S., and Duhan, V. (2018). Sphingolipids in early viral replication and innate immune activation. Biol. Chem. *399*, 1115–1123.

Carr, J.M., Mahalingam, S., Bonder, C.S., and Pitson, S.M. (2013). Sphingosine kinase 1 in viral infections. Rev. Med. Virol. *23*, 73–84.

Christofferson, D.E., and Yuan, J. (2010). Necroptosis as an alternative form of programmed cell death. Curr. Opin. Cell Biol. *22*, 263–268.

Dolnik, O., Kolesnikova, L., and Becker, S. (2008). Filoviruses: interactions with the host cell. Cell. Mol. Life Sci. *65*, 756–776.

Di Pardo, A., Amico, E., Basit, A., Armirotti, A., Joshi, P., Neely, M.D., Vuono, R., Castaldo, S., Digilio, A.F., Scalabrì, F., et al. (2017). Defective Sphingosine-1-phosphate metabolism is a druggable target in Huntington's disease. Sci. Rep. *7*, 5280.

Di Pardo, A., Pepe, G., Castaldo, S., Marracino, F., Capocci, L., Amico, E., Madonna, M., Giova, S., Jeong, S.K., Park, B.M., et al. (2019). Stimulation of sphingosine kinase 1 (SPHK1) is beneficial in a huntington's disease pre-clinical model. Front. Mol. Neurosci. *12*, 100.

Escudero-Pérez, B., Volchkova, V.A., Dolnik, O., Lawrence, P., and Volchkov, V.E. (2014). Shed GP of Ebola virus triggers immune activation and increased vascular permeability. PLoS Pathog. *10*, e1004509.

Fauci, A.S. (2014). Ebola-underscoring the global disparities in health care resources. N. Engl. J. Med. *371*, 1084–61004509.

Geisbert, T.W., Young, H.A., Jahrling, P.B., Davis, K.J., Larsen, T., Kagan, E., and Hensley, L.E. (2003). Pathogenesis of Ebola hemorrhagic fever in primate models: evidence that hemorrhage is not a direct effect of virus-induced cytolysis of endothelial cells. Am. J. Pathol. *163*, 2371–2382, https://doi.org/10.1016/S0002-9440(10)63592-4.

Hannun, Y.A., and Obeid, L.M. (2018a). Sphingolipids and their metabolism in physiology and disease. Nat. Rev. Mol. Cell Biol. *19*, 175–191.

Hannun, Y.A., and Obeid, L.M. (2018b). Author Correction: sphingolipids and their metabolism in physiology and disease. Nat. Rev. Mol. Cell Biol. *19*, 673.

Hatoum, D., Haddadi, N., Lin, Y., Nassif, N.T., and McGowan, E.M. (2017). Mammalian sphingosine

kinase (SphK) isoenzymes and isoform expression: challenges for SphK as an oncotarget. Oncotarget *8*, 36898–36929.

Hofmann, L.P., Ren, S., Schwalm, S., Pfeilschifter, J., and Huwiler, A. (2008). Sphingosine kinase 1 and 2 regulate the capacity of mesangial cells to resist apoptotic stimuli in an opposing manner. Biol. Chem. *389*, 1399–1407, https://doi.org/10.1515/BC.2008.160.

Hong, J.H., Youm, J.K., Kwon, M.J., Park, B.D., Lee, Y.M., Lee, S.I., Shin, D.M., and Lee, S.H. (2008). K6PC-5, a direct activator of sphingosine kinase 1, promotes epidermal differentiation through intracellular Ca2+ signaling. J. Invest. Dermatol. *128*, 2166–2178.

Imre, G. (2020). The involvement of regulated cell death forms in modulating the bacterial and viral pathogenesis. Int. Rev. Cell Mol. Biol. *353*, 211–253, https://doi.org/10.1016/bs.ircmb.2019.12.008.

Ji, F., Mao, L., Liu, Y., Cao, X., Xie, Y., Wang, S., and Fei, H. (2015). K6PC-5, a novel sphingosin kinase 1 (SphK1) activator, alleviates dexamethasone-induced damages to osteoblasts through activating SphK1-Akt signaling. Biochem. Biophys. Res. Commun. *458*, 568–575.

Levine, M.M. (2019). Monoclonal Antibody therapy for ebola virus disease. N. Engl. J. Med. *381*, 2365–2366, https://doi.org/10.1056/NEJMe1915350.

Liu, H., Zhang, Z., Xu, M., Xu, R., Wang, Z., and Di, G. (2018). K6PC-5 activates SphK1-nrf2 signaling to protect neuronal cells from oxygen glucose deprivation/Re-oxygenation. Cell. Physiol. Biochem. *51*, 1908–1920.

Mace, P.D., and Riedl, S.J. (2010). Molecular cell death platforms and assemblies. Curr. Opin. Cell Biol. *22*, 828–836.

Miller, M.E., Adhikary, S., Kolokoltsov, A.A., and Davey, R.A. (2012). Ebolavirus requires acid sphingomyelinase activity and plasma membrane sphingomyelin for infection. J. Virol. *86*, 7473–7483.

Newton, J., Lima, S., Maceyka, M., and Spiegel, S. (2015). Revisiting the sphingolipid rheostat: evolving concepts in cancer therapy. Exp. Cell Res. *333*, 195–200.

Obinata, H., and Hla, T. (2019). Sphingosine 1-phosphate and inflammation. Int. Immunol. *31*, 617–625.

Olejnik, J., Alonso, J., Schmidt, K.M., Yan, Z., Wang, Marzi, A., Ebihara, H., Yang, J., Patterson, J.L., Ryabchikova, E., and Mühlberger, E. (2013). Ebola virus does not block apoptotic signaling pathways. J. Virol. *87*, 5384–5396.

Ollmann Saphire, E. (2020). A vaccine against ebola virus. Cell *181*, 6, https://doi.org/10.1016/j.cell.2020.03.011.

Pourrut, X., Kumulungui, B., Wittmann, T., Moussavou, G., Délicat, A., Yaba, P., Nkoghe, D., Gonzalez, J.P., and Leroy, E.M. (2005). The natural history of Ebola virus in Africa. Microbes Infect. *7*, 1005–1014.

Pyne, N.J., El Buri, A., Adams, D.R., and Pyne, S. (2018). Sphingosine 1-phosphate and cancer. Adv. Biol. Regul. *68*, 97–106.

Reid, S.P., Tritsch, S.R., Kota, K., Chiang, C.Y., Dong, L., Kenny, T., Brueggemann, E.E., Ward, M.D., Cazares, L.H., and Bavari, S. (2015). Sphingosine kinase 2 is a chikungunya virus host factor co-localized with the viral replication complex. Emerg. Microbes Infect. *4*, e61, https://doi.org/10.1038/emi.2015.61.

Sanchez, A., Yang, Z.Y., Xu, L., Nabel, G.J., Crews, T., and Peters, C.J. (1998). Biochemical analysis of the secreted and virion glycoproteins of Ebola virus. J. Virol. *72*, 6442–6447.

Schneider-Schaulies, J., and Schneider-Schaulies, S. (2015). Sphingolipids in viral infection. Biol. Chem. *396*, 585–595.

Seo, Y.J., Pritzl, C.J., Vijayan, M., Bomb, K., McClain, M.E., Alexander, S., and Hahm, B. (2013). Sphingosine kinase 1 serves as a pro-viral factor by regulating viral RNA synthesis and nuclear export of viral ribonucleoprotein complex upon influenza virus infection. PLoS One *8*, e75005, https://doi.org/10.1371/journal.pone.0075005.

Shao, J.J., Peng, Y., Wang, L.M., Wang, J.K., and Chen, X. (2015). Activation of SphK1 by K6PC-5 inhibits oxygen-glucose deprivation/reoxygenation-induced myocardial cell death. DNA Cell Biol. *34*, 669–676.

Simmons, G., Reeves, J.D., Grogan, C.C., Vandenberghe, L.H., Baribaud, F., Whitbeck, J.C., Burke, E., Buchmeier, M.J., Soilleux, E.J., Riley, J.L., et al. (2003). DC-SIGN and DC-SIGNR bind ebola glycoproteins and enhance infection of macrophages and endothelial cells. Virology *305*, 115–123, https://doi.org/10.1006/viro.2002.1730.

Sun, L., Wang, H., Wang, Z., He, S., Chen, S., Liao, D., Wang, L., Yan, J., Liu, W., Lei, X., and Wang, X. (2012). Mixed lineage kinase domain-like protein mediates necrosis signaling downstream of RIP3 kinase. Cell *148*, 213–227.

Tewari, M., Quan, L.T., O'Rourke, K., Desnoyers, S., Zeng, Z., Beidler, D.R., Poirier, G.G., Salvesen, G.S., and Dixit, V.M. (1995). Yama/CPP32 beta, a mammalian homolog of CED-3, is a CrmA-inhibitable protease that cleaves the death substrate poly(ADP-ribose) polymerase. Cell *81*, 801–809.

Vanden Berghe, T., Linkermann, A., Jouan-Lanhouet, S., Walczak, H., and Vandenabeele, P. (2014). Regulated necrosis: the expanding network of non-apoptotic cell death pathways. Nat. Rev. Mol. Cell Biol. *15*, 135–147.

Vijayan, M., Seo, Y.J., Pritzl, C.J., Squires, S.A., Alexander, S., and Hahm, B. (2014). Sphingosine kinase 1 regulates measles virus replication. Virology *450-451*, 55–63.

Volchkov, V.E., Feldmann, H., Volchkova, V.A., and Klenk, H.D. (1998). Processing of the Ebola virus glycoprotein by the proprotein convertase furin. Proc. Natl. Acad. Sci. U S A *95*, 5762–5767.

Wolf, T., Kann, G., Becker, S., Stephan, C., Brodt, H.R., de Leuw, P., Grünewald, T., Vogl, T., Kempf, V.A., Keppler, O.T., and Zacharowski, K. (2014). Severe Ebola virus disease with vascular leakage and multiorgan failure: treatment of a patient in intensive care. Lancet *S0140-6736*, 62384–62389.

Wyllie, A.H. (1987). Apoptosis: cell death in tissue regulation. J. Pathol. *153*, 313–316.

Xia, C., Seo, Y.J., Studstill, C.J., Vijayan, M., Wolf, J.J., and Hahm, B. (2018). Transient inhibition of sphingosine kinases confers protection to influenza A virus infected mice. Antivir. Res. *158*, 171–177.

Yamane, D., Zahoor, M.A., Mohamed, Y.M., Azab, W., Kato, K., Tohya, Y., and Akashi, H. (2009). Inhibition of sphingosine kinase by bovine viral diarrhea virus NS3 is crucial for efficient viral replication and cytopathogenesis. J. Biol. Chem. *284*, 13648–13659.

iScience, Volume *24*

Supplemental information

The sphingosine kinase 1 activator,

K6PC-5, attenuates Ebola virus infection

Gergely Imre, Verena Krähling, Madeleine Eichler, Sandra Trautmann, Nerea Ferreirós, M. Javad Aman, Fatah Kashanchi, Krishnaraj Rajalingam, Stefan Pöhlmann, Stephan Becker, Dagmar Meyer zu Heringdorf, and Josef Pfeilschifter

SUPPLEMENTAL FIGURES

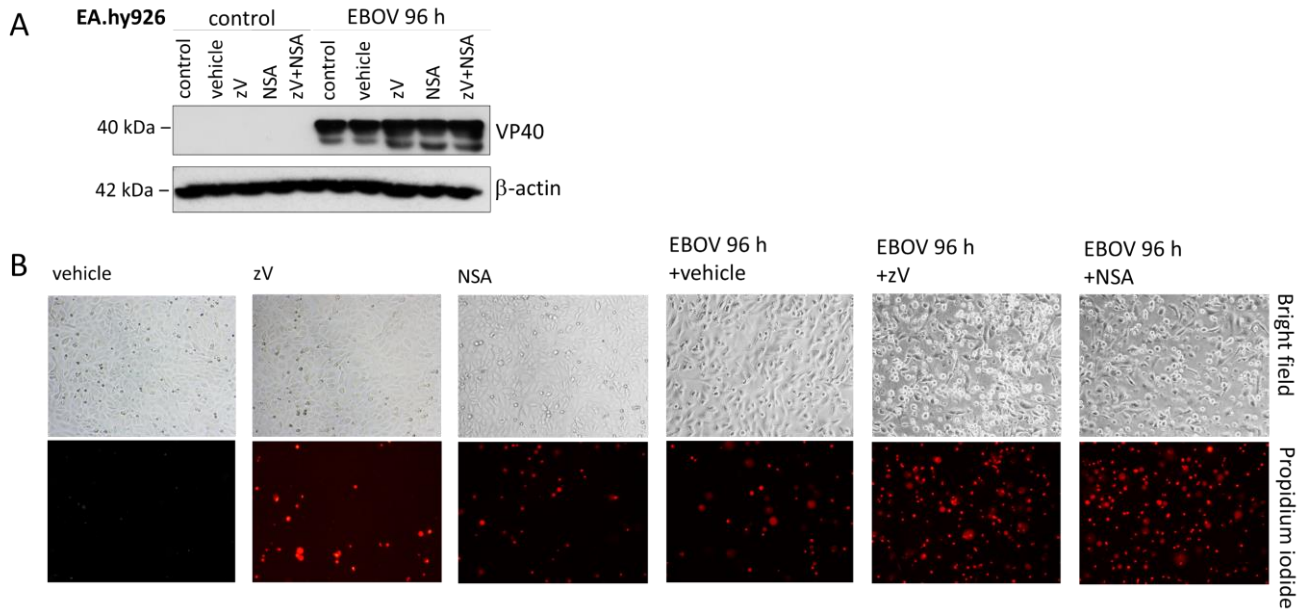

Figure S1: Treatment with zV or NSA has no influence on EBOV infection and infection induced cell death. Related to Figure 1.

(A) Immunoblot of VP40 viral matrix protein 96 h after EBOV infection in EA.hy926 cells. The cells were treated with vehicle (DMSO), 10 µM z-VAD-FMK (zV), 2 µM NSA (necrosulfonamide) or with zV in combination with NSA.

(B) Fluorescence microscopy of propidium iodide-stained EA.hy926 cells 96 h after EBOV infection (MOI=1). The cells were treated with vehicle (DMSO), 10 µM z-VAD-FMK (zV), 2 µM NSA (necrosulfonamide) or with zV in combination with NSA at 0 h. Scale bar: 50µm.

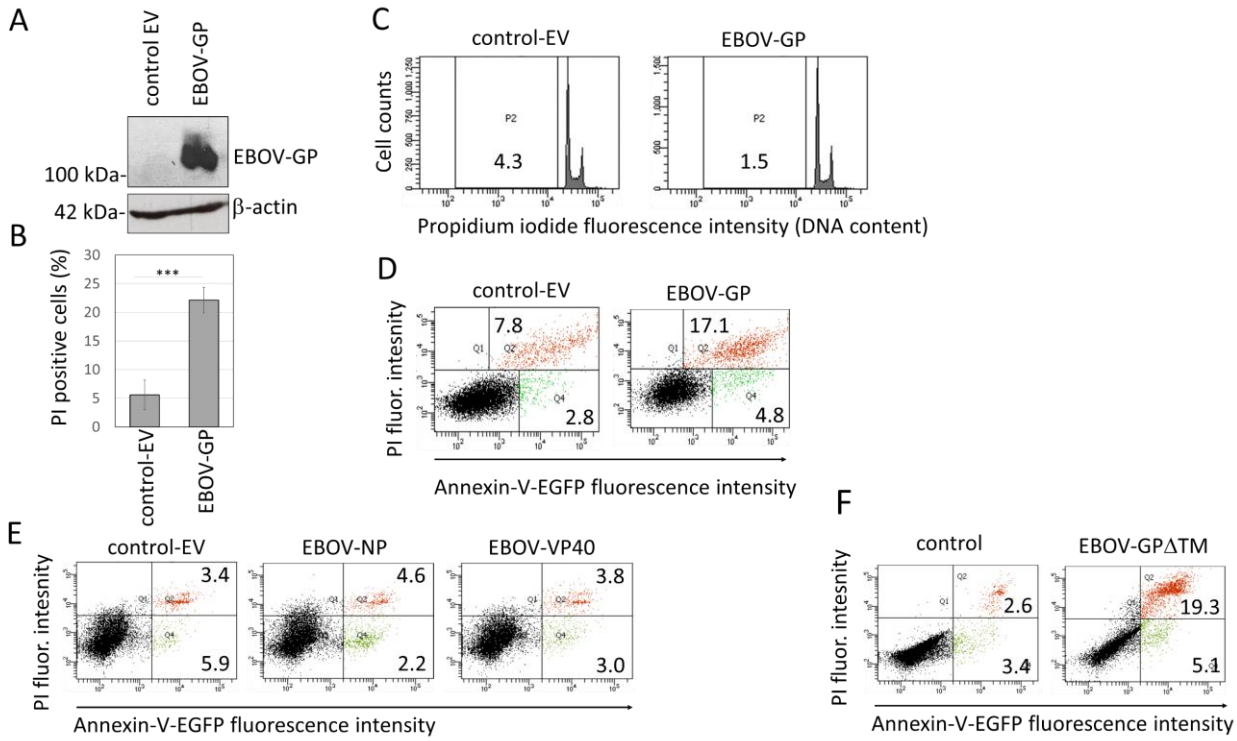

Figure S2. EBOV-GP induces necrotic cell death. Related to Figure 1.

(A) Immunoblot of EBOV-GP expressing cells. EA.hy926 cells were transfected with 1.5 µg/ml pcDNA3.1-empty vector (control EV) or pcDNA3.1-EBOV-GP and harvested for immunoblot 24 h after transfection.

(B) Percentage of propidium iodide positive EA.hy926 cells detected by flow cytometry 24 h after transfection with pcDNA3.1-empty vector (control-EV) or pcDNA3.1-EBOV-GP as in A. Data are presented as mean±SD. n=5; ***p<0.001 in Student´s t-test.

(C) Flow cytometry analysis of pcDNA3.1 empty vector (control-EV) and pcDNA3.1-EBOV-GP (EBOV-GP)-transfected EA.hy926 cells 24 h after transfection. The values indicate the percentage of apoptotic (subG1) population.

(D) Flow cytometry of EA.hy926 cells transfected with 1.5 µg/ml of pcDNA3.1-empty vector (control-EV) or pcDNA3.1-EBOV-GP. Percentage of Annexin-V-positive (green) cells and propidium iodide-Annexin-V double positive (red) cells are indicated.

(E) Flow cytometry of EA.hy926 cells transfected with 1.5 µg/ml of pcDNA3.1-empty vector (control EV), pcDNA3.1-EBOV-NP or -VP40 (24 h after transfection). Percentage of Annexin-V-positive (green) cells and propidium iodide-Annexin-V double positive (red) cells are indicated.

(F) Flow cytometry (as in D) of EA.hy926 cells treated with 40 µg/ml recombinant EBOV-GP without transmembrane domain (EBOV-GPdTM) (24 h).

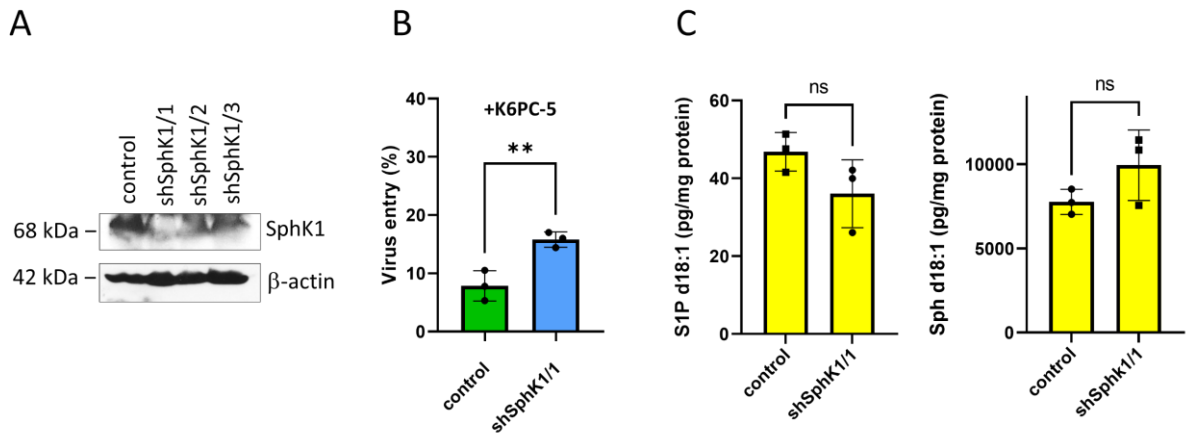

Figure S3. The effect of stable genetic depletion of SphK1 in MLV-EBOV-GP transduced cells. Related to Figure 2.

(A) Western blot analysis of EA.hy926 cells (control) and stable Sphk1 knock down EA.hy926 cells (shSphK1/1; -2; -3).

(B) Luciferase activity of K6PC-5 (25 µM) treated and MLV-EBOV-GP transduced EA.hy926 cells (control) and Sphk1 knock down EA.hy926 cells (shSphK1/1) 24 h after transduction. The values indicate the percentage of viral entry, measured as luciferase activity, relative to the vehicle (DMSO) treated samples. Data are presented as means±SD, n=3; **p<0.01 in one-sample t-test.

(C) Mass spectrometry-based determination (lower panel) of the concentration of S1P and sphingosine (Sph) d18:1 in EA.hy926 (control) and Sphk1 knock down EA.hy926 cells (shSphK1/1). The samples were normalized to total protein concentration. The values represent the amount of S1P (pg) in the relation of 1 mg total protein of the corresponding lysate. Data are shown as means±SD, n=3, ns, not significant in Student´s t-test.

TRANSPARENT METHODS

Cell lines and reagents

HeLa (American Type Culture Collection (ATCC; CCL-2)) and EA.hy926 (Edgell et al., 1983) cell lines were cultured in RPMI-1640 medium (Gibco), and HEK293T (ATCC CRL-11268) cells were cultured in DMEM (Gibco), both containing 10 % fetal bovine serum (FBS; Sigma-Aldrich) and 1 % penicillin-streptomycin (Sigma-Aldrich) and incubated at 37 °C and in 5 % CO_2. Human dermal microvascular endothelial cells (HMEC-1 cells) were from ATCC (CRL-3243) and cultured in MCDB-131 medium (Gibco) supplemented with glutamine (10 mM), epidermal growth factor (10 ng/ml), hydrocortisone (1 µg/ml), and 10 % FBS. For inhibitor experiments, cells were cultured in 6wel or 12 well plates. K6PC-5 (Sigma-Aldrich) (dissolved in dimethyl sulfoxide (DMSO)) was added to the cells in concentrations indicated in the figure legends. Sphingosine-1-Phosphate (d18:1) (S1P) (Avanti Polar Lipids) was dissolved in methanol and was added in combination with 100 ng/ml fatty acid free bovine serum albumin (BSA) (Sigma-Aldrich) to the cells at 1 µM final concentration. The solvent was used as control. Benzyloxycarbonyl-Val-Ala-Asp (OMe) fluoromethylketone (Z-VAD-fmk) (Biozol) and necrosulfonamide (Biotechne) were dissolved in DMSO and were used in concentrations indicated in the figures. $S1P_1$ agonist SEW2871 (ENZO), $S1P_2$ agonist CYM5520, and FTY720-phosphate (FTYp) (both from Cayman) were dissolved in DMSO. $S1P_{1/3}$ antagonist VPC23019 (Tocris) was dissolved in DMSO. Pertussis toxin (PTX) (Calbiochem) was dissolved in sterile ddH2O.

Virus infection and titration

The Zaire Ebola virus (EBOV) (GenBank accession number: NC_002549) was propagated in Vero C1008 cells (ATCC CRL-1586). EA.hy926 cells were pre-treated with inhibitors (specified in the figures) or with the vehicle (DMSO) one h before infection. The cells were infected with EBOV at a multiplicity of infection (MOI) of 1. After virus adsorption at 37 °C for 1 h, the inoculum was removed, cells were washed with PBS and incubated in DMEM with 2 % fetal calf serum. The inhibitors were added again in the same concentration as before the infection. Samples from the supernatant were taken at the indicated time points post infection. The samples were clarified by centrifugation for 5 minutes at 8,000 rpm and titrated onto Vero C1008 cells.

Virus titer was determined by $TCID_{50}$/ml analysis. Briefly, Vero cells were cultured in 96 well plates to 50 % confluence and infected with 10-fold serial dilutions of supernatants from infected cells. At 10 to 14 days post infection, when the cytopathic effect had stabilized, cells were analysed by light microscopy. The $TCID_{50}$/ml was calculated using the Spearman-Kärber method (Hierholzer and Killington, 1996). All work with Ebola virus was performed in the biosafety level-4 (BSL4) laboratory of the Institute of Virology, Philipps-University Marburg, Germany.

VP40 /DAPI staining immunofluorescence

Cells were washed with phosphate-buffered saline (PBS) and fixed with 4% paraformaldehyde for at least 30 min. The fixative was removed, and free aldehydes were quenched with 100 mM glycine in PBS. Afterwards, the samples were washed with PBS, the cells were

permeabilized with 0.1% Triton X-100 in PBS. The cells were incubated in blocking solution (2% bovine serum albumin, 0.2% Tween 20, 5% glycerol, and 0.05% sodium azide in PBS). and stained with a monoclonal anti-VP40 antibody (1:50). After washing steps, the cells were incubated with an anti-mouse Alexa-594 secondary antibody and co-stained with DAPI. The samples were visualized by fluorescence microscopy (Zeiss Axiomat).

Cell transfection with plasmids

Cells were cultured in 6 or 12 well plates until 70 % confluence. 100 µl/ml OptiMEM (Gibco) was mixed with GeneJuice (Merck-Millipore) (DNA : GeneJuice ratio = 1µg : 3µl) and incubated at room temperature for 5 minutes. Then, the plasmid (pcDNA3.1-empty-vector, -zEBOV-GP, -zEBOV-VP40, -zEBOV-NP, pmCherry-C1, pmCherry-C1-SphK1, pEYFP-N1 and pAcGFP-C2-hSphK2) was added to the mix, incubated for further 15 minutes and added to the cells. The cells were incubated in 5 % CO_2 at 37 °C as long as indicated in the figure legends. The cells transfected with empty vector or pmCherry-C1-SphK1 were treated with 1 mg/ml G418 (Sigma-Aldrich) 6 h after transfection for positive selection, and kept in culture for additional 6 days with complete medium change (with 1 mg/ml G418) on every second day. Six days after treatment, cells that had survived were plated on 12 well plates. On the next day, the cells were transduced with murine leukemia virus (MLV) virions as described in the section “MLV pseudotyped viral particles”. Luciferase activity detection/harvesting for immunoblot analysis was performed 24 h post infection.

Generation of stable knock down cells using lentiviral shRNA particles.

In order to achieve a stable knock down, EA.hy926 cells were seeded in 96 well plate format at 40,000 cells/100 µl medium. On the next day, the medium was changed to polybrene (hexadimethrine bromide, final concentration: 8 µg/ml) containing medium and the cells were infected with shRNA-carrying lentiviral particles (Sigma-Aldrich) at a MOI of 6. The medium was changed 24 h later. At 48 h post-infection, the cells were trypsinized, resuspended in puromycin-containing medium and seeded onto 12 well plates. To avoid clonal-specific effects, a pool of infected cells was used for the subsequent experiments after validating the knock down of the respective genes by immunoblot analysis. The following sequences of *SphK1* were employed for accomplishing knock down:

shSphk1/1 (TRCN0000344943):

CCGGACCTAGAGAGTGAGAAGTATCCTCGAGGATACTTCTCACTCTCTAGGTTTTTTG

shSphK1/2 (TRCN0000333028):

CCGGCGCTGTGCCTTAGTGTCTACTCTCGAGAGTAGACACTAAGGCACAGCGTTTTTG

shSphK1/3 (TRCN0000219838):

CCGGAGAAGGTGGAGGCTATGCTTTCTCGAGAAAGCATAGCCTCCACCTTCTTTTTTG

and

ShControl (SHC002V): non-target shRNA

Immunoblot assay

Cells seeded on 6 well plates were harvested by scratching, 50 µl 2x Laemmli (Sigma-Aldrich) was added and the samples were incubated at 99 °C for 5 minutes. 20 µl sample/ condition was subjected to SDS/PAGE. Next, the samples were transferred to a nitrocellulose membrane (0.45 µm, Biorad). The membrane was blocked for 1 h with 5 % milk or BSA TBS/0.1 % Tween at room temperature, washed three times for 5 minutes with TBS/0.1 % Tween, and then incubated with the respective primary antibody in 5 % milk TBS/0.1 % Tween overnight at 4 °C. Next, the membrane was washed three times for 5 minutes with TBS/0.1 % Tween, incubated with the corresponding horseradish peroxidase-conjugated secondary antibody for 1 h at room temperature, and washed again three times for 5 minutes. Then, the membrane was incubated 5 minutes with enhanced chemiluminescence solution (GE Healthcare), and luminescence was detected using a light sensitive X-ray film (Amersham hyperfilm, GE healthcare).

Visualization of necrotic cell death in cell culture by fluorescence microscopy

To detect necrotic cell membrane integrity loss in cell culture, cells grown in 12 well plates were incubated for 15 minutes with 2 µg/ml propidium iodide (Sigma-Aldrich). In figure 1, the propidium iodide fluorescence (excitation: 534 nm; emission: 617 nm) was imaged using a fluorescence cell culture microscope. The propidium iodide positive cells (red fluorescence) and the total number of cells (bright field) were quantified by employing the ImageJ analysis software.

Cell death detection by flow cytometry

For cell death detection, $0.5x10^6$ cells per well were seeded onto 12 well plates. After treatment as indicated in the figure legends, they were washed with 150 µl Dulbecco´s phosphate buffered saline (DPBS; Gibco) and incubated for 5 minutes with 150 µl trypsin/EDTA (Gibco). The collected cells were washed, resuspended in 300 µl resuspension buffer (ENZO) with 3 µl propidium iodide (PI) (ENZO) and 3 µl Annexin-V-EGFP (ENZO). Cells were analysed on FACSCanto-II flow cytometer (BD Bioscience) with FACSDiva, by employing the Annexin-V-EGFP/FL1 (488-nm blue laser/530-nm band-pass filter) and PI/FL2 channel (488-nm blue laser/585-nm band-pass filter). The debris (population exhibiting low FSC/FL2 intensity) was excluded from the analysis by employing the FSC/FL2 dot-plot.

Detection of the sub-G1 population by flow cytometry

The appearance of sub-G1 (under G1 phase) population of cells was monitored to measure apoptosis. Samples were prepared by employing a modified protocol of Gong et al (Gong J. et al., 1994). The treated cells were centrifuged and the pellets were resuspended in 1 ml of 70 % ethanol (−20 °C). The cells were fixed at room temperature for 30 minutes and stored at −20 °C overnight. Oligonucleosomal DNA fragments were extracted from ethanol-fixed cells in 1 ml of extraction buffer containing 200 mM Na_2HPO_4/citric acid (pH 7.8) and 10 µg/ml RNAse A (Sigma-Aldrich) for 15 min, then stained with propidium iodide (5 µg/ml final concentration) for 15 minutes before measurement. Cells were analysed on FACSCanto-II flow cytometer (BD Bioscience) with FACSDiva. Cells were gated to exclude the debris by using the FSC/FL2 dot-plot. The sub-G1 population was analysed by employing the FL2 histogram.

Production of murine leukemia virus (MLV) pseudotyped viral particles

MLV-pseudotyped viral particles were produced in HEK-293T cells. The cells were seeded onto 6 well plates with 1 ml medium per well at 70% confluence. The transfection reagent contained 100 µl/ml OptiMEM (Gibco) and 7.2 µl/ml GeneJuice (Merck-Millipore), mixed and incubated at room temperature for 5 minutes. Then, 1.2 µg/ml pTG-Luc, 0.6 µg/ml pCMV-MLV-gag-pol and 0.6 µg/ml pcDNA3.1-empty-vector (EV) or -zEBOV-GP was added, incubated for further 15 minutes and finally given to the cells. The medium was replaced 6 h post-transfection. Supernatant was harvested after 24 h, the cells were again filled up with 1 ml complete DMEM medium and harvested a second time 24 h later. The collected viral supernatant was filtered using a 0.45 µM filtertube (Merck-Millipore) and kept at -80 °C.

MLV luciferase assay

The cells were cultured in 12 well plates to 80 % confluence. After removing the supernatant, 1000 µl MLV viral supernatant was added and incubated at 37 °C and in 5 % CO_2 for 24 or 48 h. Next, the supernatant was collected, the plate was washed with 500 µl DPBS (Gibco), incubated for 5 minutes with 300 µl Trypsin-EDTA (Gibco) and the detached cells were pooled together with the collected supernatant and DPBS of the corresponding samples. The cell suspension was centrifuged at 2000 rpm for 4 minutes, the pellet was resuspended in 50 µl cell lysis buffer (Promega) and incubated for 15 minutes. After transferring the lysate into a 96 well white microplate (Corning-Costar), the luminescence intensity was detected (integration time 500 ms) before and after adding 90 µl Luciferase-reagent (Promega) by employing a SpectraMax luminometer (Molecular Devices) with SoftMax Pro software.

Sphingolipid analysis

$8x10^6$ cells were washed 2x in PBS and were harvested by scraping and mixing with 500 µl methanol (-20 °C). The protein measurement was performed parallel on a portion ($2{,}67x10^6$ cells) of the same sample by employing the Bradford method. The samples were collected in 1.5 ml tubes and the methanol was removed by employing speedvac. The sphingolipid analysis was done using liquid chromatography-electrospray ionization-tandem mass spectrometry (LC-ESI-MS/MS) as described elsewhere (Talanta, 2020). In brief, cell samples were resuspended in 200 µl extraction buffer (citric acid 30 mM, disodium hydrogen phosphate 40 mM) and mixed with 20 µl internal standard solution.

Then, the samples were extracted once with 600 µl methanol:chloroform:HCl (15:83:2, v/v/v). The collected lower organic phases were evaporated at 45 °C under a gentle stream of nitrogen and reconstituted in 50 µl methanol containing 5 % formic acid. For calibration standards and quality control samples preparation, 20 µl of the working solution were processed as stated instead of sample.

The quantification of all analytes was performed using a hybrid triple quadrupole-ion trap mass spectrometer QTRAP 5500 (Sciex, Darmstadt, Germany) equipped with a Turbo-V-source operating in positive ESI mode. Sphingolipids were separated using an Agilent 1290 HPLC system equipped with a Zorbax C8 Eclipse Plus UHPLC column (2.1 * 30 mm, 1.8 µm, Agilent technologies, Waldbronn, Germany). Quality control samples of three different concentration levels (low, middle, high) were run at the beginning and end of each run. Samples were processed using Analyst software 1.6 and the obtained concentrations were evaluated using MultiQuant 3.0 (both Sciex, Toronto, Canada) using the internal standard method (isotope-

dilution mass spectrometry). Calibration curves were calculated by linear or quadratic regression with 1/x weighting or 1/x2 weighting, respectively. Variations in accuracy of the calibration standards were lower than 15 % over the range of calibration, except for the lower limit of quantification (LLOQ), where a limit of 20 % was accepted.

Statistical analysis

Student`s t test, one way ANOVA or one sample t test was performed to test for statistical significance of the results as indicated in the corresponding figure legends. (*P≤0.05, **P≤0.01, ***P≤0.001, ****P≤0.*0001*, ns= not significant). The sample size (number of independent experiments) is indicated in the figure legends as *n=x*.

REAGENT or RESOURCE	SOURCE	IDENTIFIER
Antibodies		
α-tubulin	Sigma-Aldrich	
α-Beta-Actin-Mouse Monoclonal (AC-15)	Sigma-Aldrich	Lot#026M4780V
α-SphK1-Mouse	Abnova	H000056848B01P
α-SphK2-Mouse	Abnova	H00008877-M01
Living colors	Clontech	632377
α-mCherry	Abcam	#43590
α-Mouse-HRP IgG Goat	Sigma-Aldrich	#12349
α-PARP 46D11 Rabbit mAb	Cell Signaling	#9532
α-Rabbit-HRP IgG Goat	Sigma-Aldrich	#A0545
α-zEBOV-GP 4F3 Mouse mAb	IBT Bioservices	Lot#1501002
α-zEBOV-VP40 Rabbit pAb	IBT Bioservices	Lot#1107001S
Plasmids		
pcDNA3.1	Invitrogen	
pmCherry-C1	Clontech/Takara Bio Europe France	
pEYFP-N1	Clontech	
pmCherry-C1_Sphk1	described in Blankenbach et al. 2020	NCBI reference sequence NM_001142601.2
pcDNA3.1_zEBOV-GP	Prof. Dr. Fatah Kashanchi	
pcDNA3.1_zEBOV-NP	Prof. Dr. Fatah Kashanchi	

pcDNA3.1_zEBOV-VP40	Prof. Dr. Fatah Kashanchi	
pCMV-MLV-gag-pol	Prof. Dr. Pöhlmann	Bartosch B. et al., 2003
pTG-luc	Prof. Dr. Pöhlmann	Bartosch B. et al., 2003
pAcGFP-C2_SphK2	A. Don & H. Rosen	Addgene plasmid #84370
Cell lines		
EA.hy926	Prof. Dr. Pfeilschifter	Edgel J. et. al., 1983
HEK-293T	ATCC	CRL-11268
HeLa	ATCC	CCL-2
HMEC-1	ATCC	CRL-3243
Viruses		
Zaire Ebola virus (EBOV)	Prof. Dr. Stephan Becker	GenBank accession number NC_002549
Chemicals, Commercial Assays		
Amersham ECL Western Blotting Detection Reagents	GE Healthcare	Lot#16809358
Annexin V-EGFP Apoptosis Detection Kit	ENZO	Lot#08081911
GeneJuice Transfection Reagent	MERCK-Millipore	Lot#3248274
z-VAD-fmk	Biozol	APE-A1902-1MG
Necrosulfonamide	Biotechne	5025/10
K6PC-5	Sigma-Aldrich	SML1709
CYM5520 (CYM)	Cayman	1449747-00-5
SEW2871 (SEW)	Enzo Life Sciences	BML-LPI06-0050
FTY720-phophate (FTYp)	Cayman	10008639
VPC23019 (VPC)	Tocris	4195
Pertussis toxin (PTX)	Calbiochem	516560
Sphingosine-1-Phosphate (d18:1) (S1P)	Avanti Polar Lipids	860492
Luciferase Assay System	Promega	Lot#000392448
Propidium iodide solution	Sigma-Aldrich	Lot#MKBV9923V
Sample Buffer Laemmli 2x Concentrate	Sigma-Aldrich	Lot#SLBX2653
Software and Algorithms		
FACSDiva	BD Bioscience	

SoftMaxPro	Molecular Devices	
ImageJ	ImageJ	https://imagej.nih.gov/ij/
GraphPad Prism 9.0.0	GraphPad Software	http://graphpad.com

SUPPLEMENTAL REFERENCES

Gong, J., Traganos, F., Darzynkiewicz Z. (1994). A selective procedure for DNA extraction from apoptotic cells applicable for gel electrophoresis and flow cytometry. Anal Biochem. 218, 314–319.

Hierholzer JC., Killington RA. (1996) Virus isolation and quantitation. In: Kangro BW., Ma HO., editor. Virology methods manual. London, United Kingdom: Academic Press Limited. 36–38.

Talanta, J. (2020). Implementation of lipidomics in clinical routine: Can fluoride/citrate blood sampling tubes improve preanalytical stability? 209, 120593. doi: 10.1016/j.talanta.2019. 120593. Epub 2019 Nov 26.